A Study of Cysteamine Ionization in Solution by Raman Spectroscopy and Theoretical Modeling

Laurynas Riauba,*,† Gediminas Niaura,‡ Olegas Eicher-Lorka,‡ and Eugenijus Butkus†

Department of Organic Chemistry, Vilnius University, Naugarduko 24, LT-03225 Vilnius, Lithuania, and Institute of Chemistry, Goštauto 9, LT-01108 Vilnius, Lithuania

Received: June 19, 2006; In Final Form: October 5, 2006

Different cysteamine ($H_2N-CH_2-CH_2-SH$) ionization forms have been studied by polarized Raman spectroscopy in solutions prepared with H_2O and D_2O and by DFT calculations at the B3LYP/6-31++G(d,p) level. To account for solvation effects, we employed the integral equation formalism polarizable continuum model (IEFPCM) option and explicit water molecules. Calculated relative energies and Raman spectra revealed that *gauche* rotamers around the C−C bond are the most stable conformers in solution. The experimental pK_a values and Raman spectra of various ionization forms were best predicted by using a model with three explicit water molecules and the IEFPCM option. In general, the use of IEFPCM tends to lower the calculated frequencies for a few bands, but in some cases (S−H stretching mode) this effect is expressed very strongly. Potential energy distribution (PED) analysis of *gauche* conformers of various cysteamine ionization forms provided the possibility of discriminating spectroscopically methylene groups adjacent to sulfur, $(CH_2)_S$, and nitrogen, $(CH_2)_N$, sites. In general, stretching and scissoring modes as well as wagging and twisting vibrations of the $(CH_2)_N$ group were found to be at higher frequencies. The influence of ionization of SH and NH_2 groups on the vibrational spectrum is discussed, and Raman markers for further amine group ionization studies are suggested.

1. Introduction

Cysteamine (2-aminoethanethiol) is a small bifunctional molecule that is used widely as a chelating ligand in coordination chemistry,[1,2] biochemistry,[3,4] and for construction of functional self-assembled monolayers (SAMs) on metal surfaces.[5−9] Its SH group forms a strong metal−sulfur chemical bond upon adsorption on gold,[10] silver,[11] and copper[12] surfaces, whereas the NH_2 group interacts with ions,[12−14] organic molecules,[15] and proteins[16,17] in the solution phase used to prepare molecular structures with specific properties. Ionization and solvation of the amine group in aqueous solutions controls the binding properties of the cysteamine linkage to the solution-phase species. To construct the surface layers with desired physicochemical properties, understanding of the structure of cysteamine monolayers at molecular level is required. Vibrational spectroscopic techniques, in particular surface-enhanced Raman spectroscopy (SERS), are able to provide the required microscopic information on the structure of the interface.[12−14,16,18−21] However, because of extended vibrational coupling and the influence of ionization of ending groups, the interpretation of the surface vibrational spectrum is not straightforward, and in general cannot be accomplished without the high level of computational modeling. The first step in such studies is related to the understanding of the solvation and vibrational properties of the studied compound in aqueous solutions, and the second step is associated with modeling of the surface complex. The Raman spectra of cysteamine in solution were reported previously, and some bands were assigned.[12,18,22,23] Thus, Nandy et al. [22] assigned the 663 and 760 cm^{-1} C−S stretching bands to *gauche* and *trans* rotational conformers, respectively. Similarly, the CCN deformation peak at 391 cm^{-1} was attributed to the *gauche* conformer, whereas the higher frequency component at 452 cm^{-1} was associated with the same vibrational mode of the *trans* conformer.[22] In SERS-related studies, the solution and surface Raman spectra of cysteamine were compared and a red shift of C−S stretching band upon adsorption of thiol on silver[18] and copper[12] surfaces was evidenced. Raman spectra of 2 M cysteamine hydrochloride in the wide frequency region were reported recently by Fleischer at al.[23] They demonstrated the disappearance of the S−H stretching peak at 2577 cm^{-1} upon addition of one equivalent of NaOH. However, internal vibrations of cysteamine were not analyzed in detail. Thus, in spite of the importance of cysteamine in coordination and surface chemistry, and the potential applicability of vibrational spectroscopy in determining *in situ* the structure of the compound and the state of the functional groups, the reported Raman studies are based on the empirical assignments of the bands. To fully exploit Raman signals, reliable assignments of even lower intensity bands, spectroscopic discrimination between two CH_2 groups (adjacent at sulfur and nitrogen sites), and evaluation of the ionization state and conformation-sensitive modes are required. It should be noted that the parameters (frequency, bandwidth, and relative intensity) of nearly all of the cysteamine bands in Raman spectra are highly affected by the ionization state of the SH and NH_2 groups. In addition, the normal modes of cysteamine are complex mixtures of C−C and C−N stretching, CH_2 bending, twisting, wagging, and rocking, and NH_2/NH_3^+ bending vibrations. Consequently, an unambiguous assignment of the cysteamine vibrational modes is rather complicated. The reliable way of determining the identity of vibrational modes is via quantum mechanical analysis coupled with isotopic substitution experimental studies and measure-

* To whom correspondence should be addressed. E-mail: laurynas.riauba@chf.vu.lt.
† Vilnius University.
‡ Institute of Chemistry.

10.1021/jp063816g CCC: $33.50
Published on Web 11/30/2006

ments of depolarization ratios of Raman bands. Several studies devoted to the computational analysis of cysteamine appeared previously.[23−25] Thus, an ab initio quantum chemical study of cysteamine at the HF/6-31G(d) level using an Onsager self-consistent reaction field ($\epsilon = 78.39$) showed that the zwitterionic structure is energetically more stable compared to the uncharged form because of dipolar solute−solvent and hydrogen-bonding interaction.[23] Colson and Sevilla[24] have calculated the cysteamine aqueous-phase ionization energies at the ROHF/6-31G* level in order to understand the radioprotective capability of the thiol toward oxidative DNA ion radicals. An ab initio study of the conformational behavior of the uncharged cysteamine molecule in vacuum at the MP2/6-31G** level revealed a weak hydrogen bond S−H···N responsible for the stabilization of the *gauche* conformer.[25] However, no theoretical analyses of the vibrational spectra of various cysteamine ionization forms were accomplished in the above-discussed studies.

With this in mind, we focused in this work on the theoretical modeling and Raman spectroscopic study of various ionization forms of cysteamine in aqueous solutions prepared with water and deuterated water. To the best of our knowledge, no theoretical investigations for vibrations of cysteamine as well as experimental Raman depolarization ratio measurements were reported.

Because of the importance of the interaction of charged groups with water molecules, the theoretical models used for the calculation of the vibrational spectrum should account for the solvation effects. Reliable solvation models must lead to an accurate prediction of cysteamine pK_a values. Various solvation models might be applied, and most of them use the continuum solvation approach. The history of and theory behind continuum solvation models have been laid out exclusively in various articles.[26−29] The most prevailing of them are polarized continuum models (PCM).[26,30−32] Three main different approaches exist to exercise PCM calculations, namely, dielectric PCM (D-PCM), the second model that treats the surrounding medium as a conductor instead of a dielectric (C-PCM) and, finally, the integral equation formalism implementation of PCM (IEF-PCM).[33,34] Very similar to PCM is the conductor-like screening model (COSMO),[35−38] which is also quite current and widely implemented in software packages. However, there are solvation models attempting to take into account solvent effects by adding explicit solvent molecules.[39] Although these models are much more computationally expensive, they can provide insight into many fundamental issues[40,41] or can improve ionization constant (pK_a) prediction accuracy.[42] Effects of the solvent on vibrational spectra are discussed less considerably. Some continuum models were applied successfully.[43−48] Stefanovich and Truong[49] used the COSMO model to calculate the vibrational shifts of five molecules in water and demonstrated that the addition of one explicit water molecule greatly improved the results for substances like formic and acetic acid, which form strong hydrogen bonds with water. Tajkhorshid et al.[50] concluded that the calculated vibrational properties of L-alanine could be significantly influenced by very small rearrangements in the relative position of the neighboring water molecules in the first hydration shell, but overall calculated spectra were in good agreement with experimental ones.

In this work, we have combined theoretical modeling, including polarizable continuum models and explicit water molecules, and polarized Raman spectroscopy for the study of different ionization forms of cysteamine in solution prepared with water and deuterated water. At first we analyzed the effect of various solvation models on the calculated energies and pK_a values, and then Raman spectra were investigated. Raman bands were assigned on the basis of experimentally determined depolarization ratios, deuteration shifts, and PED analysis. The influence of ionization of SH and NH_2 groups as well as the solvation model on the vibrational spectrum is discussed. Finally, Raman bands, which may serve as vibrational markers for ionization studies of the NH_3^+ group are proposed.

2. Models and Calculation Methods

When modeling cysteamine solution in water, the following aspects have to be considered. Cysteamine exists in three ionic forms: the positively charged form ($Cyst^+$), the zwitterionic form (Cyst-ZW), and the negatively charged form ($Cyst^-$). Computational models for all of these ionic forms were developed.

For all of the following models with the positively charged form of cysteamine, the formal charge was considered to be +1 and the spin multiplicity was considered to be 1. For all models with the zwitterionic form, the charge was set to 0, and spin multiplicity to 1, whereas for the negative form models the charge was set to −1 and spin multiplicity to 1. The cysteamine molecule exists in two main conformations, *gauche* and *trans*. In a solution, the cysteamine molecule is surrounded by a quite large number of water molecules, which cannot be modeled straightforward using ab initio methods. Models containing zero, one, two, and three water molecules were evaluated. All of the calculations were performed using Gaussian for Windows package version G03W.[51] Geometry optimization and frequency calculations were accomplished with the DFT method using the B3LYP functional. Almost all of the calculations were done using the 6-31++G(d,p) basis set. Calculations using other basis sets will be indicated. To take the solvent into account, some calculations were done using the polarizable continuum model (PCM), specifically the integral equation formalism model, further referenced as IEFPCM.

Cysteamine's two ionization steps are expressed by following reactions:

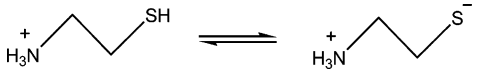

or

$$AH_2^+ \leftrightarrows AH + H^+ \quad (1)$$

and

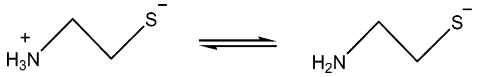

or

$$AH \leftrightarrows A^- + H^+ \quad (2)$$

The following equations are valid for these reactions:

$$\Delta E(1) = E_{AH}^{solv} + E_{H^+}^{solv} - E_{AH_2^+}^{solv} \text{ and } \Delta E(2) = E_{A^-}^{solv} + E_{H^+}^{solv} - E_{AH}^{solv} \quad (3)$$

where $E_X^{solv} = E_X + E_X(\text{solvation})$ and E_X is energy of species (this might be energy of formation or Gibbs free energy of formation or bulk electronic energies, depending on the assumptions used). If we assume that $\Delta G \approx \Delta E$ and knowing that $\Delta G = -RT \ln K$ and $pK_a = \Delta G/2.303RT$, then $\Delta G(2) - \Delta G(1) = [pK_a(2) - pK_a(1)]/2.303RT$. Also, using the same

assumptions, $E^{solv}_{H^+} = 0.5(E^{solv}_{AH_2^+} - E^{solv}_{A^-} + [pK_a(1) + pK_a(2)]/2.303RT)$ or $E^{solv}_{H^+} = E^{solv}_{AH_2^+} - E^{solv}_{AH} + [pK_a(1)]/2.303RT$ or $E^{solv}_{H^+} = E^{solv}_{AH} - E^{solv}_{A^-} + pK_a(2)/2.303RT$.

Vibrational frequencies and the Raman spectra line intensities were calculated using the Gaussian 03W package.[51] Usually calculated harmonic frequencies tend to overestimate or underestimate the observed frequencies in a systematic manner[52−54] due to the neglect of anharmonicity and incomplete treatment of electron correlation. Multiplication of calculated frequencies by some scaling factor, which depends on the calculation method selected, is considered an ordinary procedure. Use of more sophisticated correction procedures can greatly improve the agreement between the calculated and observed frequencies.[52,54−57] The following relation can be defined: $\nu' = a(\nu)\cdot\nu$, where a(ν) is scaling factor, which depends on frequency. In the simplest case, the scaling factor linearly depends on frequency. Assuming that for a certain frequency calculated and the experimental data are almost equal and denoting this frequency as ν^0, for some frequency ν^F scaling factor can be defined as a^F. Usually this factor varies between 0.9 and 1 and frequency ν^F can be chosen arbitrarily, for example, as the upper limit of the calculated spectra. Then $a(\nu)$ can be expressed as follows:

$$a(\nu) = 1 - (1 - a^F)\frac{\nu - \nu^0}{\nu^F - \nu^0} \tag{4}$$

All of the following calculated frequencies were scaled using parameters: $a^F = 0.97$, $\nu^F = 3000$, and $\nu^0 = 600$. The calculated Raman intensities of our studied models have a tendency to have higher intensities at high frequencies; therefore, generated spectra at lower frequencies are less representative than higher frequency parts. To enhance clearness, the generated Raman spectra can be further improved by scaling the calculated Raman intensities. We have used the log intensity scaling factor, which inversely depends on the logarithm of the peak frequency:

$$I'_R(\nu_n) = I_R(\nu_n)\frac{1}{\log(\nu_n)} \tag{5}$$

where $I_R(\upsilon_n)$ is the calculated Raman intensity of the nth vibration with frequency υ_n, $I'_R(\upsilon_n)$ is scaled intensity. After the scaled vibrational frequencies and scaled Raman intensities are calculated, the simulated Raman spectra can be modeled using Gaussian or Lorenzian lineshapes.

3. Experimental Section

Raman measurements were carried out in 90° scattering geometry. The 413.1 nm beam of the Kr-ion laser (Coherent, Model: Innova 90-K) was used as the excitation source. The laser power at the sample was typically 60−90 mW. The laser plasma lines were attenuated by means of an interference filter. The Raman scattering light was analyzed with a 400 mm focal length, f/2.5 spectrograph equipped with a 1200 lines/mm grating and detected by a thermoelectrically cooled (203 K) CCD camera (Princeton Instruments, Model: Spec-10:256E). A holographic filter (Kaiser Optical Systems, Model: HNPF 413.1−1.0) was placed in front of the entrance slit of the spectrograph to eliminate Rayleigh scattering from the sample. To remove the effects of the optical elements of the spectrometer on the intensities of polarized Raman spectra, a polarization scrambler was put in front of the entrance slit. The Raman frequencies were calibrated using the toluene spectrum. The integration time was 1 s. Each spectrum was recorded by accumulation of 200 scans. The overlapped bands were digitally decomposed into the components of mixed Gaussian−Lorentzian shape. The solvent spectrum was digitally subtracted from the sample spectrum.

Cysteamine hydrochloride (98%) and deuterium oxide were purchased from Sigma-Aldrich Chemie GmnH and used without further purification. The Millipore purified (18.2 MΩ cm) water was used throughout all of the experiments.

4. Results and Discussion

4.1. Molecular Structures of Cysteamine. Structures of positively charged forms of cysteamine with zero water molecules did not change considerably from the initially suggested form during geometry optimization. In models that contained water molecules, the main changes occurred on the water molecule(s) positions and orientations. Usually before optimization randomly placed water molecules did not form hydrogen bonds. After geometry optimization, water molecules were placed to form at least one hydrogen bond with cysteamine or other water molecules. It appeared that the preferred positions to form hydrogen bonds with cysteamine are hydrogen atoms of the amino group. The situation is quite different considering the neutral form. If models with zero or one water molecules are evaluated, it does not matter whether the starting geometry is neutral or zwitterionic; the final geometry is always neutral. This fact is in concordance with the experimental data for similar molecules in the gaseous phase.[58,59] If the model includes two or more water molecules, then the zwitterionic form is preferred. As can be suggested, the negatively charged sulfur atom readily forms hydrogen bonds with water molecules. The final structures involve water molecules, which are oriented so that there are two hydrogen bonds with the cysteamine molecule, that is, sulfur atom to hydrogen atom of water and from oxygen to hydrogen of the positively charged amino group so that there can be an imaginable ring containing the following atoms: $N_1-C-C-S\cdots H-O\cdots H-N_1$ (N_1 is the nitrogen atom from the amino group, and ⋯ denotes hydrogen bonds) (Figure 1). Evaluation of *trans* conformations shows similar patterns. The main difference is the absence of a stabilizing ring. Structures optimized using the polarizable continuum model formalism are quite similar to structures obtained by regular optimizations. However, there is one exception, that is, the neutral form. As mentioned above, regular optimizations without or with one water molecule yield the neutral form. Using IEFPCM options for optimizations, the zwitterionic form is formed and this result conforms to structures with few water molecules. This fact can be explained by stabilization of charges through the solvation.

4.2. Calculated Energies and Thermodynamic Properties of Cysteamine. The relative energies of the *trans* rotamer around the C−C bond are given in Table 1. For the negatively charged structures, the *gauche* form has lower energy compared to the *trans* form. Depending on a number of water molecules, the difference varies from 5 to 27 kJ/mol. Differences between the relative energies of the neutral form are quite large. Even the choice of the most stable conformation depends on a number of water molecules. Similar patterns can be observed for the positively charged form (relative energies between 1 and 23 kJ/mol). Generally speaking, the relative energy of the *trans* conformation compared with the *gauche* conformation is lower for the structures with more water molecules included. The obtained relative Gibbs free energies can differ from the calculated relative electronic energy by ±10 kJ/mol. Calculations with bigger basis sets 6-311++(d,p) were also performed (Table 1). The absolute energies calculated using this basis set are quite different from the energies calculated with the 6-31G++(d,p)

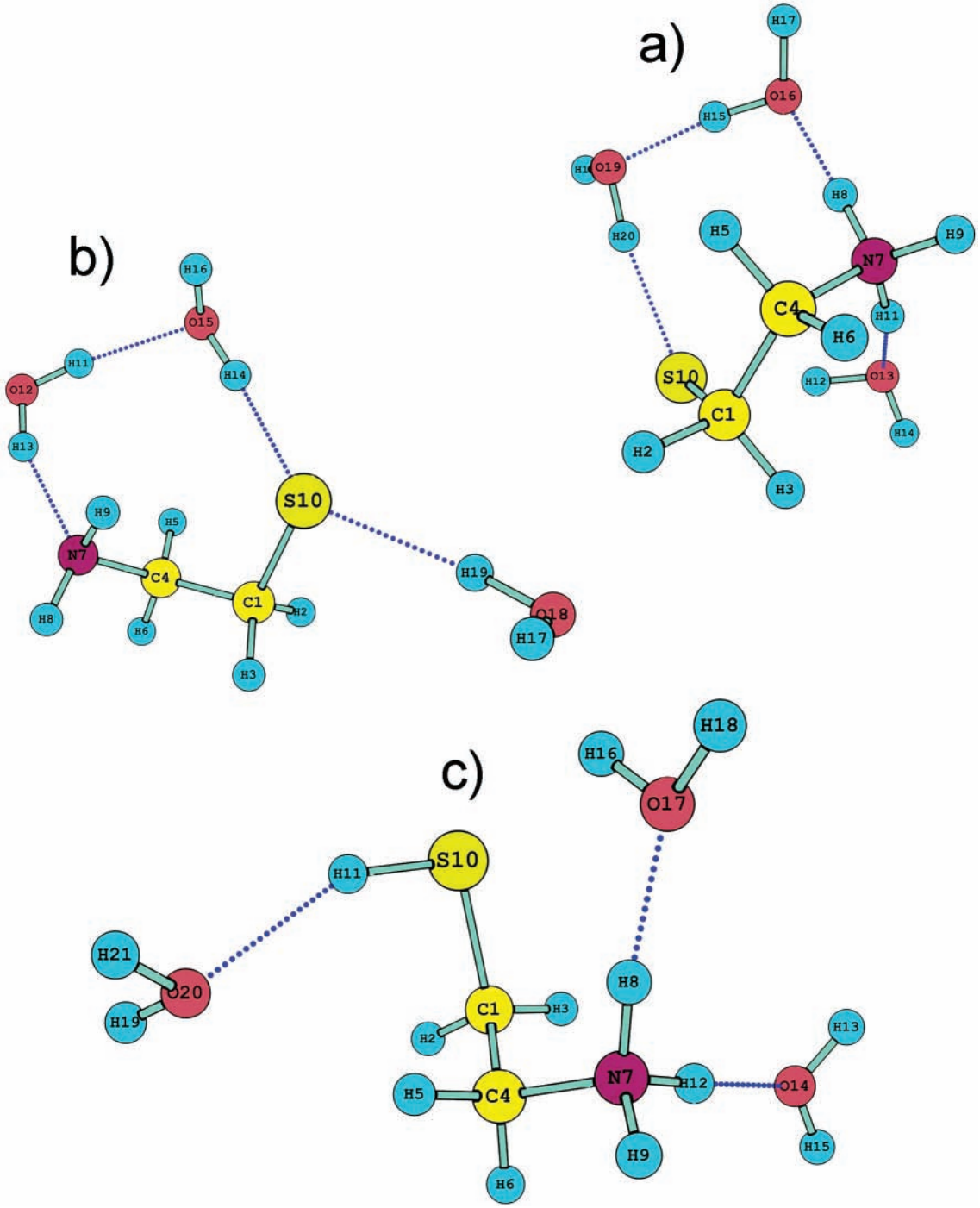

Figure 1. Calculated structures of cysteamine: (a) zwitterionic form (total charge 0) with three water molecules, (b) negatively charged form (total charge −1) with three water molecules, and (c) positively charged form (total charge +1) with three water molecules.

basis set. Despite this fact, calculations using larger basis sets principally yield the same result. The difference between relative energies calculated using 6-31G++(d,p) and 6-311++(d,p) basis sets are less than 0.6 kJ/mol.

Results of solvation calculations are given in Table 2. Experimentally determined dissociation constant values were found to be $pK_{a1} = 8.32$ and $pK_{a2} = 10.81$[60,61] for first and second ionization stages, respectively. Differences between the first and second ionization stage dissociation constants are best predicted using the polarizable continuum model. It seems that the number of water molecules included in the model does not significantly affect the calculated pK_a difference. Although results obtained using absolute energies with zero-point correction are improved compared to results gained using calculated free Gibbs energies, it is unclear whether it is the systematic trend or the accidental result. Models that were employed without using the IEFPCM option resulted in quite large errors in pK_a difference calculations and the models with fewer water molecules resulted in larger errors. This fact is not surprising knowing that water solvates cysteamine molecules, lowering the energy of the charged species.

Calculations of proton hydration free energies by combining experimental pK_a values and calculated internal energies yielded average values between −1127 and −1142 kJ/mol, whereas values referenced in the literature vary between −1090 and −1105 kJ/mol for Gibbs free energy and −1130 to −1150 kJ/

TABLE 1: Relative Energies (in kJ/mol) of *Trans* as Compared with *Gauche* Rotational Conformers around the C−C Bond of Cysteamine

		energy			
charge	number of water molecules	electronic	sum of electronic and zero-point	Gibbs free	difference, G−E
−1	0	18.510	17.302	16.370	−2.140
−1	1	23.100	25.145	26.999	3.899
−1	2	4.884	7.678	16.443	11.559
−1	3	15.196	10.062	5.504	−9.692
0	0	39.853	35.872	25.836	−14.017
0	1	26.398	23.882	16.102	−10.296
0	2	83.897	83.127	77.983	−5.914
0	3	−2.203	−2.348	−2.907	−0.704
+1	0	22.950	21.934	20.172	−2.778
+1	1	20.177	19.153	17.431	−2.746
+1	2	15.514	15.729	12.132	−3.382
+1	3	−8.655	−4.987	1.347	10.002
+1	1[a]	20.022	18.948	17.108	−2.914
+1	2[a]	16.097	16.333	12.785	−3.312
+1	3[a]	−8.508	−4.703	2.059	10.567

[a] Calculations were performed using the 6-311++(d,p) basis set.

mol for enthalpy values. Again, the proton solvation energy values obtained without the IEFPCM option and from individual ionization constants tend to be very scattered.

The best results for the prediction of cysteamine dissociation constants were found by using complexes with three water molecules and the IEFPCM option and by employing electronic energy with zero-point correction (Table 2).

4.3. Vibrational Spectroscopy. We have measured the parallel and perpendicular polarized Raman spectra of cysteamine in various media. The following solutions were used: (i) 1 M cysteamine hydrochloride in water and in deuterated water, (ii) 1 M cysteamine hydrochloride in 1 M NaOH solution and the same composition in deuterated water, and (iii) 1 M cysteamine hydrochloride in 2 M NaOH solution and the same composition in deuterated water. Interpretation of Raman spectra was based on previous vibrational studies of related compounds,[12,18,22,23,50,62−64] depolarization ratios experimentally observed in this work, and theoretical modeling of cysteamine clusters with different numbers of water molecules as well as by using IEFPCM option. Because models with zero and one water molecule cannot reproduce the zwitterionic form, for further vibrational analysis complexes with three water molecules and the IEFPCM option will be primarily discussed.

Stretching Vibrations of Ionizable Groups. Figure 2 compares the experimental and calculated Raman spectra of cysteamine at different ionization states observed in solutions prepared with D_2O in the S−D and N−D stretching frequency region. We present the spectra of deuterated samples to avoid interference with C−H stretching modes and, moreover, this provides the possibility of directly monitoring the ionization state of SD and ND_3^+ groups. The strong and relatively sharp ν(S−D) band at 1872 cm^{-1} indicates the presence of the S−D bond for 1 M cysteamine/D_2O solution. It should be noted that the experimental 1872 cm^{-1} peak is asymmetric and contains a shoulder on the lower frequency side. Decomposition of the spectral contour into the mixed Gaussian−Lorentzian components yields

TABLE 2: Calculation of Solvation Energy and pK_a

model, energy	$\Delta\Delta G$ (kJ/mol)	ΔpK_a	$E(H^+,solv)$ (kJ/mol)	$E(H^+,solv)^a$ (kJ/mol)	$E(H^+,solv)^b$ (kJ/mol)	pK_a(1)	pK_a(2)
0 water molecules, Gibbs free energy	−545.1	−95.5	−1127.8	−862.5	−1393.2	−33.3	62.2
1 water molecule, Gibbs free energy	−437.7	−76.7	−1133.1	−921.3	−1344.8	−30.0	46.7
2 water molecules, Gibbs free energy	−281.4	−49.3	−1131.3	−997.7	−1264.9	−16.6	32.7
3 water molecules, Gibbs free energy	−291.6	−51.1	−1128.7	−990.0	−1267.4	−18.0	33.1
0 water molecules, Gibbs free energy, IEFPCM option	−9.0	−1.5	−1138.8	−1141.5	−1136.2	8.6	10.1
0 water molecules, electronic energy with zero-point correction, IEFPCM option	−11.0	−2.0	−1138.0	−1139.6	−1136.3	8.2	10.2
0 water molecules, enthalpy, IEFPCM option	−12.8	−2.3	−1137.1	−1137.8	−1136.4	7.9	10.2
3 water molecules, Gibbs free energy, IEFPCM option	−7.6	−1.3	−1142.1	−1145.4	−1138.8	9.3	10.6
3 water molecules, electronic energy, IEFPCM option	−41.5	−7.3	−1165.2	−1151.5	−1178.8	10.3	17.6
3 water molecules, enthalpy, IEFPCM option	−16.8	−3.0	−1139.2	−1138.0	−1140.5	7.9	10.9
3 water molecules, electronic energy with zero-point correction, IEFPCM option	−14.1	−2.5	−1140.9	−1441.0	−1140.8	8.3	10.8
experimental[60,61]		−2.49				8.32	10.81

[a] Proton solvation energies calculated using only first ionization stage. [b] Proton solvation energies calculated using only second ionization stage.

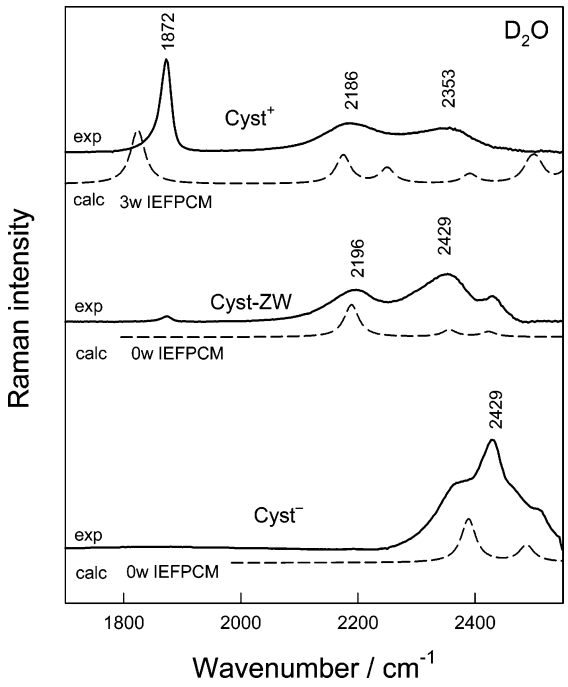

Figure 2. Experimental and calculated Raman spectra of different ionization forms of cysteamine in the S−D and N−D stretching frequency region. Experimental spectra were observed in 1 M cysteamine hydrochloride solution prepared with D_2O and containing different amounts of NaOH. The solvent spectrum was subtracted. The following models with deuterated water and deuterons at N and S sites were used: 0w IEFPCM, model with zero water molecules, gauche form, IEFPCM option; 3w IEFPCM, model with three water molecules, gauche form, IEFPCM option.

two polarized S−D stretching bands located at 1857 [full width at half-maximum (fwhm) was found to be 39 cm^{-1}] and 1873 cm^{-1} (fwhm = 19 cm^{-1}) (Figure S1, Supporting Information). The corresponding modes are shifted to 2555 (fwhm = 56 cm^{-1}) and 2579 cm^{-1} (fwhm = 25 cm^{-1}), respectively, in 1 M cysteamine/H_2O solution (Figure S2). We attributed the broad lower frequency component to the ν(S−D)/ν(S−H) mode of strongly hydrogen-bonded through the S−D/S−H group $Cyst^+$ species. The model with three water molecules reproduces the experimental S−H frequency well (Table 3). However, for the IEFPCM option without water molecules the calculated frequency was found to be at 2309 cm^{-1}, considerably lower than the experimental value. A similar result can be obtained for the model of the *trans* conformation of $Cyst^+$ with three water molecules and the IEFPCM option; the calculated frequency of ν(S−H) is 2332 cm^{-1}. It is worth noting that for both models hydrogen from the SH group does not have water molecules in proximity. The calculated frequency of the ν(S−H) band for the model with three water molecules and the IEFPCM option (Table 3) was slightly lower (2521 cm^{-1}) than the experimental frequency. These results can be explained assuming that the IEFPCM method overestimates S−H solvation (especially when the S−H group does not have explicit solvating water molecules nearby) and therefore calculated frequencies are lower than the experimental frequencies. Calculations from models that do not include explicit water molecules and the IEFPCM option yield frequencies of approximately 2610 cm^{-1}. It should be noted that models that reproduced experimental S−H frequency best had at least one water molecule near the S−H group (distance between H and O atoms is in the range 2.1 to 2.4 Å). Thus, analysis of the S−H stretching mode should treat the IEFPCM results with care, and the effects of solvation by including explicit water molecules should be accounted. In general, the ν(S−H) frequency is best predicted with models including three explicit water molecules.

Two broad features at 2186 (fwhm = 127 cm^{-1}) and 2353 cm^{-1} (fwhm = 119 cm^{-1}) in the experimental spectrum of $Cyst^+$ (Figure 2) represent the stretching vibrations of the ND_3^+ group. The spectral parameters of the higher frequency component cannot be determined unambiguously because of interference with the water band. However, the lower frequency component is clearly expressed and based on polarization measurements ($\rho = 0.09$) this band was attributed to the symmetric stretching vibration, $\nu_s(ND_3)$. In H_2O solution, this band shifted to 3113 cm^{-1} (Table 3). Calculations performed with the 3w IEFPCM model reproduces vibrations of the positively charged ND_3^+ group well (Figure 2). The calculated $\nu_s(ND_3)$ for the $Cyst^+$ form was found to be at 2175 cm^{-1}. Experimental spectra in Figure 2 show that upon addition of 1 M sodium hydroxide to 1 M cysteamine/D_2O, the characteristic $\nu_s(ND_3)$ band is visible at 2196 cm^{-1}, whereas the ν(S−D) band at 1872 cm^{-1} disappears, demonstrating the presence of a positively charged amine group and formation of a dominant zwitterionic cysteamine form in the studied solution. Calculations performed with the 0w IEFPCM model for the Cyst-ZW form reproduces the $\nu_s(ND_3)$ band at 2189 cm^{-1} (Figure 2). In the spectrum of 1 M cysteamine/D_2O solution containing 2 M sodium hydroxide, the $\nu_s(ND_3)$ band disappears and an intense $\nu_s(ND_2)$ feature at 2429 cm^{-1} (fwhm = 47 cm^{-1}) grows up, indicating deprotonation of the ammonium group and transformation of the cysteamine species from the zwitterionic to anionic form. It should be noted that the $\nu_s(ND_2)$ band was found to be considerably narrowed as compared with the $\nu_s(ND_3)$ mode. In excellent agreement with the experimental spectrum, calculations performed with the 0w IEFPCM model for the $Cyst^-$ form showed a considerable increase (by 200 cm^{-1}) in N−D symmetric stretching frequency upon transformation of the ND_3^+ group to ND_2.

C−H Stretching Vibrations. Figure 3 shows the experimental Raman spectra of cysteamine at different ionization states in the frequency region of the C−H stretching vibration observed in solutions prepared with H_2O or D_2O. The calculated spectra of deuterated compounds at nitrogen and sulfur sites for various ionization states and solvation models are displayed in Figure 4. The experimental and calculated Raman wavenumbers along with the experimental depolarization ratios (ρ) and assignments for positively and negatively charged cysteamine models, respectively, are summarized in Tables 3 and 4. The frequency of C−H stretching vibrations is sensitive to the ionization state of the amine group. As can be seen from Figure 3, for the positively charged amine group the high-frequency ν(C−H) component is detected in the vicinity of 2967−2976 cm^{-1}. Upon deprotonation, this band shifts to lower wavenumbers by ~20−50 cm^{-1}, resulting in the broad feature at ~2920 cm^{-1}. This phenomenon was discussed extensively in the previous works dedicated to the vibrational studies of amino acids and short-chain hydrocarbons containing amine groups.[64−67] It should be noted that this high-frequency component is clearly polarized and the degree of depolarization increases markedly when the NH_3^+ group loses a proton (Figure 3, Tables 3 and 4). First, the assignments of the C−H bands based on polarization measurements and model calculations are discussed. The calculations provide a basis for differentiation of methylene groups at sulfur $(CH_2)_S$ and nitrogen $(CH_2)_N$ sites. The highly polarized 2906 and 2953 cm^{-1} bands of the $Cyst^+$ ion (Figure 3) was immediately assigned to $\nu_s(CH_2)_S$ and $\nu_s(CH_2)_N$ modes, respectively (Table 3). Symmetric $(CH_2)_N$ frequency appears

TABLE 3: Raman Experimental and Calculated Wavenumbers (in cm^{-1}), Experimental Depolarization Ratios, and Approximate Descriptions of Cysteamine Positively Charged Model Vibrations

experimental		calculated			
wavenumbers	ρ	3 water molecules, *gauche* (Figure 1c)[a]	0 water molecules, *gauche*, IEFPCM option	3 water molecules, *gauche*, IEFPCM option[a]	approximate description
390 m	0.23	444	437	477	δ(CCN)
641 w, sh	0.24				ν(C−S), strongly hydrogen-bonded
663 vs	0.18	649	645	647	ν(C−S)
780 m	0.12	780	764	787	r$(CH_2)_S$ + δ(CSH)
813 w	0.08		844	889	δ(CSH) + δ(CNH)
870 w	0.26	883	870	895	ν_s(C−C−N) + δ(CSH)
901 m	0.63	901			r$(CH_2)_N$ + r(NH_3)
945 m	0.18		943		δ(CNH) + r(NH_3)
990 w	0.33	995		1007	δ(CNH) + δ(CSH)
1023 m	0.71	1021	1017	1038	ν_{as}(C−C−N)
1044 m	0.59	1108	1058	1101	$\delta(NH_3)$ + δ(CCH)
1133 w	0.71	1152	1116	1147	δ(CSH) + t$(CH_2)_S$
1254 m	0.64	1263	1244	1255	t$(CH_2)_S$
1281 m	0.27	1312	1291	1302	wag$(CH_2)_S$
1331 m	0.69	1346	1332	1344	t$(CH_2)_N$
1388 m	0.29	1404	1396	1398	wag$(CH_2)_N$
1430 m	0.77	1449	1434	1441	$\delta(CH_2)_S$
1464 m	0.73	1493	1467	1477	$\delta(CH_2)_N$
			1481		$\delta_s(NH_3)$
			1589	1567	$\delta(NH_3)$
1620 m	0.91	1670	1596	1647	$\delta_{as}(NH_3)$
		1692		1687	$\delta_{as}(NH_3)$
2556 s, sh	0.17				ν(S−H), strongly hydrogen-bonded
2578 vs	0.11	2570	2309	2521	ν(S−H)
2906 s	0.02	2988	2964	2965	$\nu_s(CH_2)_S$
2953 vs	0.03	2976	2973	2976	$\nu_s(CH_2)_N$
2969 s	p				$\nu_s(CH_2)_N$FR
2990[b] m, br	0.70	3024	3021	3024	$\nu_{as}(CH_2)_S$
		3048	3033	3043	$\nu_{as}(CH_2)_N$
3113 m	0.11	3072	3154	3233	$\nu_s(NH_3)$
		3381	3206		$\nu_{as}(NH_3)$
			3214		$\nu_{as}(NH_3)$

[a] Vibrations of solvated water molecules are not included. [b] Wavenumber determined from perpendicularly polarized spectrum. Abbreviations: ρ, depolarization ratio; p, polarized; m, middle, w, weak; s, strong; vs, very strong; ν, stretching; ν_s, symmetric stretching; ν_{as}, asymmetric stretching; δ, deformation; δ_s, symmetric deformation; δ_{as}, asymmetric deformation; r, rocking; wag, waging; t, twisting; sh, shoulder, not well-resolved band; $(CH_2)_S$ and $(CH_2)_N$ are methylene groups adjacent to S and N atoms, respectively.

at slightly higher wavenumbers. The same tendency holds for the $Cyst^-$ ion (Table 4). However, the calculated C−H symmetric stretching frequencies for the negative anion are lower by ∼50−120 cm^{-1} as compared with positively charged species and are in excellent agreement with the experiment where the downward shift by ∼70 cm^{-1} was detected. Considering the C−H asymmetric stretching bands for the $Cyst^-$ ion, we have assigned two depolarized overlapped features at 2920 and 2950 cm^{-1} (Figure 3) to $\nu_{as}(CH_2)_S$ and $\nu_{as}(CH_2)_N$ modes, respectively (Table 4). Again, the higher frequency in the calculated spectra where the solvent influence was modeled by three water molecules and for the model without water corresponds to the vibration of the $(CH_2)_N$ group. It should be noted that considerable coupling between $\nu_{as}(CH_2)_S$ and $\nu_{as}(CH_2)_N$ modes was obtained for the structure calculated within the IEFPCM option. In the case of the $Cyst^+$ ion, the depolarized (ρ = 0.7) asymmetric CH_2 vibrational mode was identified at 2990 cm^{-1} in the perpendicularly polarized experimental spectrum (Figure 3, Table 3). This feature is rather broad (fwhm = 51 cm^{-1}) and clearly integrates two vibrational bands. We associate both asymmetric, $\nu_{as}(CH_2)_S$ and $\nu_{as}(CH_2)_N$, modes to the experimental 2990 cm^{-1} band (Table 3). All of the calculated models suggest a higher C−H asymmetric frequency for the $(CH_2)_N$ group (Table 3). The highly polarized band at 2969 cm^{-1} does not have a calculated equivalent (Figure 3). We suggest that this mode belongs to the C−H symmetric stretching vibration in Fermi resonance (FR) with a CH_2 bending overtone. Most likely, it corresponds to vibration of the $(CH_2)_N$ group because an overtone of the $\delta(CH_2)_N$ mode (Table 3) appears at a closer frequency (2928 cm^{-1}) compared with the $\delta(CH_2)_S$ overtone (2860 cm^{-1}). As can be seen from the experimental spectrum (Figure 3), this mode clearly shifts upon deprotonation of the NH_3^+ group.

The trend in shifts of calculated C−H stretching frequencies for various solvation models upon transformation of the ND_2 group to ND_3^+ is demonstrated in Figure 4. We chose deuterated samples at N and S sites and solvated D_2O molecules to avoid spectral interferences of C−H vibrations with O−H and N−H stretching modes. The shift of all of the bands to lower wavenumbers is clearly visible. The presented data provide evidence for the importance of electronic effects for the C−H frequency shift upon protonation of the amine group. However, we were able to determine an experimentally small but observable shift of C−H frequency from 2969 to 2976 cm^{-1} for the $Cyst^+$ form, and from 2967 to 2970 cm^{-1} for the Cyst-ZW form, respectively, on deuteration at the N site (Figure 3). This

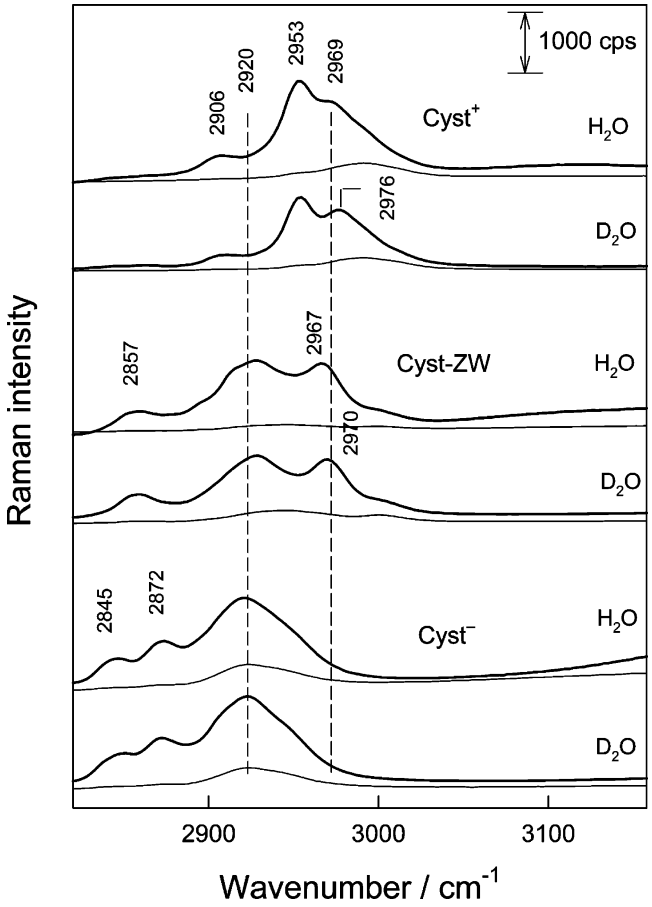

Figure 3. Experimental Raman spectra in the C−H stretching frequency region of different ionization forms of 1 M cysteamine hydrochloride in aqueous solutions containing different amounts of NaOH and prepared from H_2O or D_2O. The solvent spectrum was subtracted. Thick and thin lines represent parallel and perpendicular polarized Raman spectra, respectively.

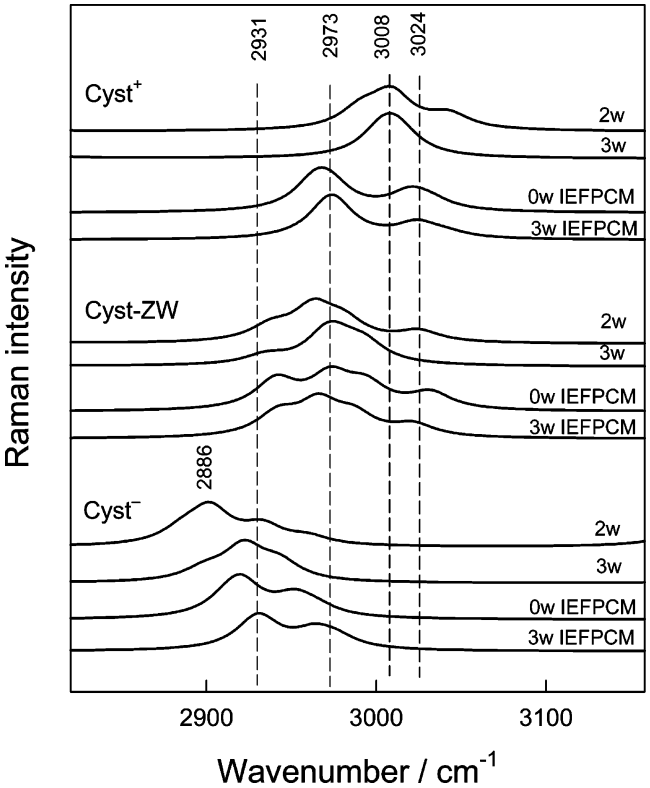

Figure 4. Calculated Raman spectra of cysteamine at different ionization states in the C−H stretching frequency region. The following models with deuterated water and deuterons at N and S sites were used: 2w, model with two water molecules, gauche form; 3w, model with three water molecules, gauche form; 0w IEFPCM, model with zero water molecules, gauche form, IEFPCM option; 3w IEFPCM, model with three water molecules, gauche form, IEFPCM option.

observation implies that not only the changes in electronic structure but also the structure of the solvent affects the stretching C−H frequency of the $Cyst^+$ and Cyst-ZW forms. We suggest that the high-frequency C−H stretching band in the vicinity of 2970 cm^{-1} observed for the $Cyst^+$ and Cyst-ZW forms may serve as a vibrational marker for the ionization studies of the NH_3^+ group. It should be noted that Raman bands associated with the vibrations of the NH_3^+ group are usually weak and broad[62] and thus not very appropriate for direct monitoring of the ionization state of the amine group. The suggested C−H mode at 2970 cm^{-1} might be a useful alternative in ionization investigations, for example, of cysteamine adsorbed at metal surfaces.

Middle Frequency Spectral Region (300−1690 cm^{-1}). Figure 5 compares the polarized experimental Raman spectra of cysteamine at different ionization states in the 300−1690 cm^{-1} spectral region observed in solutions prepared with H_2O and D_2O. The calculated spectra are displayed in Figure 6. The low-intensity polarized peak at 510 cm^{-1} does not have counter parent in calculated spectra and thus belongs to the S−S stretching vibration, indicating the presence of a small amount of disulfide cysteamine in all of the studied solutions. The most intense peak in each spectrum belongs to the highly polarized C−S stretching vibration. Its frequency is sensitive to *gauche*/*trans* rotational isomerization around the C−S bond.[12,16−21] In general agreement with calculated energies (Table 1), the experimental Raman spectra provide evidence that the *gauche* conformation (rotational isomer around the C−C bond) is the most stable form of cysteamine in aqueous solutions. In the case of the $Cyst^+$ ion, the *gauche* and *trans* C−S stretching bands appeared at 663 and 763 cm^{-1}, respectively. The calculated intensity ratio (I_G/I_T) was found to be 4.0, indicating that the *gauche* conformer dominates in solutions of positively charged cysteamine. The relative concentration of *trans* conformers increases markedly upon deprotonation of SH (I_G/I_T = 2.2 for Cyst-ZW) and NH_3^+ (I_G/I_T = 1.3) groups. The position of the $\nu(C-S)_G$ band depends slightly (within 10 cm^{-1}) on the ionization state of cysteamine. It was detected at 666 and 656 cm^{-1} for Cyst-ZW and $Cyst^-$ forms, respectively. More sensitive to ionization state is the $\nu(C-S)_T$ band (the frequency varies within 17 cm^{-1}) observed at 764, 752, and 747 cm^{-1} in $Cyst^+$, Cyst-ZW, and $Cyst^-$ solutions, respectively. Both $\nu(C-S)_G$ and $\nu(C-S)_T$ modes are sensitive to isotopic H_2O/D_2O solution exchange and, in general, exhibit a negative deuteration shift $\Delta = \nu(D_2O) - \nu(H_2O)$. Again, Δ values are considerably higher for *trans* (within −19 cm^{-1}) as compared with the *gauche* (within −5 cm^{-1}) mode. All models are very good for the prediction of the C−S bond vibration frequency (Figure 6). In the case of the $Cyst^+$ ion, the calculated frequencies are lower by ∼14−18 cm^{-1}. For zwitterion models with two and three water molecules and the IEFPCM option, we found a calculated frequency of 660 cm^{-1} (lower by 6 cm^{-1} as compared with the experimental value), whereas the model with three water molecules and the IEFPCM option yielded 643 cm^{-1} (Table S3, Supporting Information). Calculations with the IEFPCM option predict well experimentally observed lowering of the ν-(C−S) frequency by 10 cm^{-1} upon deprotonation of the NH_3^+ group (Figure 6).

TABLE 4: Raman Experimental and Calculated Wavenumbers (in cm^{-1}), Experimental Depolarization Ratios, and Approximate Descriptions of Cysteamine Negative Form Model Vibrations

experimental		calculated			
wavenumbers	ρ	0 water molecules, *gauche*	3 water molecules, *gauche* (Figure 1b)[a]	0 water molecules, *gauche*, IEFPCM option	approximate description
401 m	0.23	458	466	448	δ(CCN)
656 vs	0.15	648	650	640	ν(C−S)
824 m	0.04	820	828	818	$r(CH_2)_N + r(CH_2)_S$
896 w	0.54	887	900	867	ν(C−C−N) + $r(CH_2)_N$
		930	946	909	$r(CH_2)_S + r(CH_2)_N + \delta$(HCS)
1016 w	0.34	1018	1027	998	ν_s(C−C−N) + wag(NH_2)
1063 m	0.30	1048	1047	1053	ν(C−N) + $t(CH_2)_S$
1130 w	0.87	1117	1134	1116	$t(CH_2)_N + t(NH_2)$
1234 m	0.07	1198	1199	1206	$t(CH_2)_S$
1271 vs	0.08	1265	1269	1268	$wag(CH_2)_S + t(NH_2)$
1354 m	0.40	1344	1361	1356	$wag(CH_2)_N$
1384 w	0.15	1373	1364	1360	$t(CH_2)_N + t(NH_2)$
1436 s	0.59	1442	1451	1444	$\delta(CH_2)_S$
1463 m, sh	0.70	1455	1470	1452	$\delta(CH_2)_N$
1596 m	0.87	1636	1621	1599	$\delta(NH_2)$
2845 s	0.08	2845	2898	2908	$\nu_s(CH_2)_S$
2872 s	0.06	2869	2914	2920	$\nu_s(CH_2)_N$
2920 vs	0.21	2887	2940	2952	$\nu_{as}(CH_2)_S$, $\nu_s(CH_2)$FR
2950 m, sh	0.44	2951	2972	2965	$\nu_{as}(CH_2)_N$
3301 vs	0.06	3280	3282	3274	$\nu_s(NH_2)$
3365 m-w, sh	0.60	3365	3400	3347	$\nu_{as}(NH_2)$

[a] Vibrations of solvent water molecules are not included. Abbreviations: ρ, depolarization ratio; m, middle; w, weak; s, strong; vs, very strong; ν, stretching; ν_s, symmetric stretching; ν_{as}, asymmetric stretching; δ, deformation; δ_s, symmetric deformation; δ_{as}, asymmetric deformation; r, rocking; wag, waging; t, twisting; sh, shoulder, not well-resolved band; $(CH_2)_S$ and $(CH_2)_N$ are methylene groups adjacent to S and N atoms, respectively.

The polarized low-frequency band at 390 cm^{-1} ($Cyst^+$) is sensitive to isotopic H_2O/D_2O exchange ($\Delta = -24$, -17, and -22 cm^{-1} for $Cyst^+$, Cyst-ZW, and $Cyst^-$ forms, respectively), does not depend on ionization of the SH group (390 and 388 cm^{-1} for $Cyst^+$ and Cyst-ZW, respectively), and is sensitive to ionization of the NH_2 group (401 and 388 cm^{-1} for $Cyst^-$, and Cyst-ZW, respectively) (Figure 5). This band was attributed to the symmetric deformation vibration of the CCN chain (Tables 3 and 4). Although being rather low intensity, this mode may serve as a useful vibrational marker for studies of NH_2 group ionization.

We assigned the rocking vibration of CH_2 groups to the middle intensity polarized peak in the vicinity of 780−824 cm^{-1} (Figure 5). This mode appears at clearly lower wavenumbers for the $Cyst^+$ (780 cm^{-1}) ion as compared with the Cyst-ZW (817 cm^{-1}) and $Cyst^-$ (824 cm^{-1}) forms (Tables 3, S3, and 4). Thus, the peak in the vicinity of 817 cm^{-1} might be used as a marker band for analysis of deprotonation of the SH group.

Frequencies in the region between 850 cm^{-1} and 1200 cm^{-1} consist of a complex mix of angle bending and C−C−N stretching vibrations. For the $Cyst^+$ form, the low-intensity polarized vibration at 870 cm^{-1} (Table 3) was assigned to the ν_s(C−C−N) mode, whereas the ν_{as}(C−C−N) vibration was found to contribute to the middle intensity depolarized experimental peak at 1023 cm^{-1}. Upon ionization of the SH group, the ν_s(C−C−N) band was not clearly identified, whereas the ν_{as}(C−C−N) mode shifted to 1013 cm^{-1} (Table S3).

The spectral region between 1200 and 1400 cm^{-1} contains twisting and wagging bands of methylene groups. Vibrations of CH_2 groups adjacent to sulfur and nitrogen atoms can be clearly differentiated. In general, the wagging and twisting modes of the $(CH_2)_N$ group appear at higher wavenumbers (Tables 3 and 4).

The experimentally observed depolarized doublet in the vicinity of 1430−1465 cm^{-1} (Figure 5) belongs to the bending (scissoring) mode of the CH_2 groups. PED analysis provides the basis for differentiation of the CH_2 groups; the lower frequency component is associated with the $(CH_2)_S$ group, whereas the higher frequency band is associated with $(CH_2)_N$ (Tables 3 and 4, and Tables S2−S4). In accordance with this interpretation is a shift of the $\delta(CH_2)_S$ band frequency from 1430 to 1436−1440 cm^{-1} upon deprotonation of the SH group (Figure 5, Tables 3 and 4). For the $Cyst^-$ ion, the experimentally observed splitting of $\delta(CH_2)$ modes was reproduced well only by models containing three water molecules (3w, and 3w IEFPCM models) (Figure 6). It should be noted that the calculated $\delta(CH_2)$ frequencies for the $Cyst^-$ ion increase by 8−18 cm^{-1} for the 3w IEFPCM model as compared with models without water molecules (Table 4). The same tendency holds for the $Cyst^+$ ion (Table 3).

Comparison of the calculated frequencies to the experimental ones reveals that all methods with explicit or implicit solvent water treatment are correct. The least time-consuming model with no explicit water molecules but with the IEFPCM option shows very good results for peak frequency predictions, but the most comparable to the experimental spectra result is obtained when using the model with three water molecules and the IEFPCM option. It should be noted that models with the IEFPCM option and three water molecules predict the best experimentally observed splitting of the deformation methylene modes and the ionization-induced shifts of the C−S stretching mode.

5. Summary and Conclusions

We present the first combined theoretical and Raman spectroscopic study on different ionization forms of cysteamine in aqueous solution. DFT calculations at the B3LYP/6-31++G-(d,p) level of theory including various continuum models and explicit water molecules were employed to simulate the effect

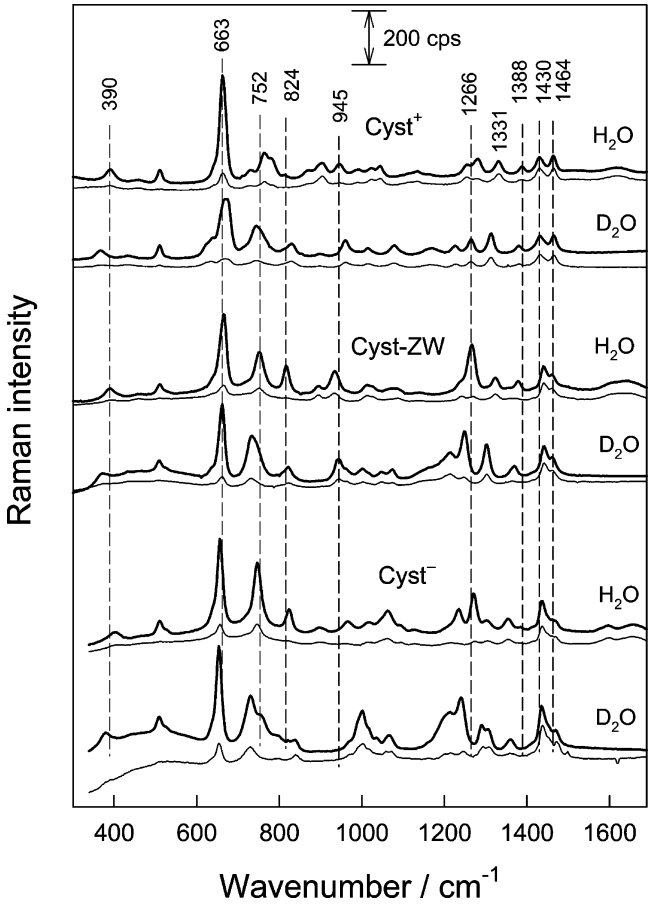

Figure 5. Experimental Raman spectra in the 300−1690 cm^{-1} spectral region of different ionization forms of 1 M cysteamine hydrochloride in aqueous solutions containing different amounts of NaOH and prepared from H_2O or D_2O. The solvent spectrum was subtracted. Thick and thin lines represent parallel and perpendicular polarized Raman spectra, respectively.

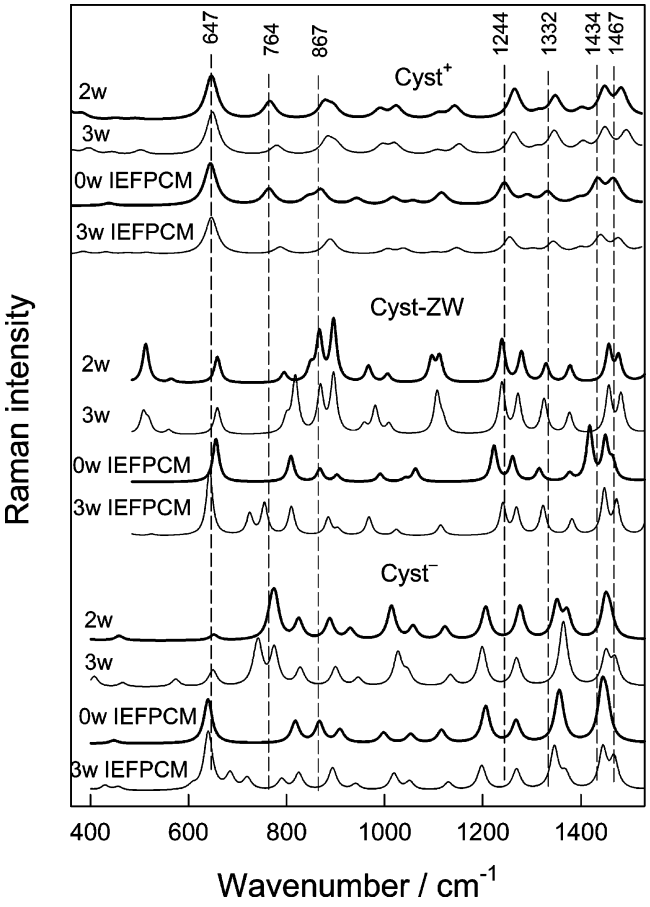

Figure 6. Calculated Raman spectra of cysteamine at different ionization states in the middle frequency region. The following models were used: 2w, model with two water molecules, gauche form; 3w, model with three water molecules, gauche form; 0w IEFPCM, model with zero water molecules, gauche form, IEFPCM option; 3w IEFPCM, model with three water molecules, gauche form, IEFPCM option.

of solvent on cysteamine ionization. The calculated energies of cysteamine conformations show that the *gauche* rotamer around the C−C bond usually is more stable than the *trans* conformation. It was found that difference in relative energy decreases with increasing number of water molecules in the complexes. The cysteamine solvation energy and experimental pK_a values of ionization of SH and NH_2 groups are best predicted using complexes with three explicit water molecules and IEFPCM (integral equation formalism polarizable continuum model) option and employing energy with zero-point correction.

Comparison of calculated and experimental Raman spectra recorded at various cysteamine ionization stages in H_2O and D_2O solutions, analysis of PED, and experimental depolarization ratios led to the assignment of vibrational bands. We have focused in this work on vibrational analysis of *gauche* conformers, the most stable form of cysteamine in aqueous solutions. The most accurate predictions are done using models with explicit water molecules and using IEFPCM formalism for calculations. It should be noted that the predicted frequencies for some bands are lowered when using IEFPCM formalism. This effect might be very strong for the S−H stretching band when there are no explicit water molecules in vicinity of this group. The S−H stretching vibration is best predicted with models including three explicit water molecules. On the basis of PED analysis, we were able to differentiate CH_2 groups at sulfur, $(CH_2)_S$, and nitrogen, $(CH_2)_N$, sites. Both the deformation (scissoring) and stretching modes of the $(CH_2)_N$ group appeared at higher frequencies as compared with $(CH_2)_S$. The same tendency holds for twisting and wagging modes. An increase in the C−H stretching frequency in the vicinity of 2970 cm^{-1} by 3−7 cm^{-1} upon H_2O exchange to D_2O was detected experimentally for Cyst-ZW and $Cyst^+$ ions, suggesting the influence of the water structure near the charged ammonium group on the stretching vibration of the $(CH_2)_N$ group.

For further Raman spectroscopic studies of NH_2 group ionization, we suggest using the following vibrational markers: the high-frequency C−H stretching band in the vicinity of 2970 cm^{-1} observed for positively charged and zwitterionic forms of cysteamine, and the symmetric deformation vibration of the CCN chain at 380−400 cm^{-1}.

Supporting Information Available: Details of PED calculation, calculated energies of models, tables with PED analysis of $Cyst^+$, Cyst-ZW, and $Cyst^-$ forms, and molecular structure coordinates of optimized structures. This material is available free of charge via the Internet at http://pubs.acs.org.

References and Notes

(1) Fleischer, H.; Dienes, Y.; Mathiasch, B.; Schmitt, V.; Schollmeyer, D. *Inorg. Chem.* **2005**, *44*, 8087.

(2) Bharara, M. S.; Parkin, S.; Atwood, D. A. *Inorg. Chem.* **2006**, *45*, 2112.

(3) Schilling, S.; Cynis, H.; von Bohlen, A. Hoffmann, T.; Wermann, M.; Heiser, U.; Buchholz, M.; Zunkel, K.; Demuth, H. U. *Biochemistry* **2005**, *44*, 13415.

(4) Liquier, J.; Fort, L.; Nguyen Dai, D.; Cao, A.; Taillandier, E. *Int. J. Biol. Macromol.* **1983**, *5*, 89.
(5) Arias, F.; Godinez, L. A.; Wilson, S. R.; Kaifer, A. E.; Echegoyen, L. *J. Am. Chem. Soc.* **1996**, *118*, 6086.
(6) Katz, E.; Shabtai, V. H.; Willner, I.; Rau, H. K.; Haehnel, W. *Angew. Chem., Int. Ed.* **1998**, *37*, 3253.
(7) Molinero, V.; Calvo, E. J. *J. Electroanal. Chem.* **1998**, *445*, 17.
(8) Willner, I.; Shabtai, V. H.; Katz, E.; Rau, H. K.; Haehnel, W. *J. Am. Chem. Soc.* **1999**, *121*, 6455.
(9) Zhang, J.; Welinder, A. C.; Hansen, A. G.; Christensen, H. E. M.; Ulstrup, J. *J. Phys. Chem. B* **2003**, *107*, 12480.
(10) Wirde, M.; Gelius, U.; Nyholm, L. *Langmuir* **1999**, *15*, 6370.
(11) Hatchett, D. W.; Uibel, R. H.; Stevenson, K. J.; Harris, J. M.; White, H. S. *J. Am. Chem. Soc.* **1998**, *120*, 1062
(12) Bloxham, S.; Eicher-Lorka, O.; Jakubėnas, R.; Niaura, G. *Spectrosc. Lett.* **2003**, *36*, 211.
(13) Mosier-Boss, P. A.; Boss, R. D. Lieberman, S. H. *Langmuir* **2000**, *16*, 5441.
(14) Michota, A.; Kudelski, A.; Bukowska, J. *J. Raman Sectrosc.* **2001**, *32*, 345.
(15) Katz, E.; Schmidt, H.-L. *J. Electroanal. Chem.* **1993**, *360*, 337.
(16) Wong, L. S.; Vilker, V. L.; Yap, W. T.; Reipa, V. *Langmuir* **1995**, *11*, 4818.
(17) Albrecht, T.; Li, W. W.; Ulstrup, J.; Haehnel, W. Hildebrandt, P. *ChemPhysChem.* **2005**, 961.
(18) Kudelski, A.; Hill, W. *Langmuir* **1999**, *15*, 3162.
(19) Michota, A.; Kudelski, A.; Bukowska, J. *Langmuir* **2000**, *16*, 10236.
(20) Michota, A.; Kudelski, A.; Bukowska, J. *Surf. Sci.* **2002**, *502*−503, 214.
(21) Wrzosek, B.; Bukowska, J.; Kudelski, A. *J. Raman Spectrosc.* **2005**, *36*, 1040.
(22) Nandy, S. K.; Kastha, G. S. *Indian J. Phys.* **1973**, *47*, 763.
(23) Fleischer, H.; Dienes, Y.; Mathiasch, B.; Schmitt, V.; Schollmeyer, D. *Inorg. Chem.* **2005**, *44*, 8087.
(24) Colson, A. O.; Sevilla, M. D. *J. Phys. Chem.* **1994**, *98*, 10484−10491.
(25) Buemi, G. *J. Quantum Chem.* **1996**, *59*, 227.
(26) Tomasi, J.; Persico, M. *Chem. Rev.* **1994**, *94*, 2027.
(27) Rivail, J.-L.; Rinaldi, D. In *Computational Chemistry, Review of Curent Trends*; Leszczynski, J., Ed.; World Scientific: New York, 1995; p 139.
(28) Cramer, C. J.; Truhlar, D. G. In *Reviews in Computational Chemistry*; Lipkowitz, K. B., Boyd, D. B., Eds.; VCH: New York, 1995; Vol. 6, p 1.
(29) Cramer, C. J.; Truhlar, D. G. In *Solvent Effects and Chemical Reactivity*; Tapia, O., Betra'n, J., Eds.; Kluwer: Dodrecht, 1996; p 1.
(30) Bagyan, G. A.; Valeev, A. K.; Koroleva, I. K.; Soroka, N. V. *Russ. J. Inorg. Chem.* **1983**, *28*, 1142.
(31) Cammi, R.; Tomasi, J. *J. Comput. Chem.* **1995**, *16*, 1449.
(32) Amovilli, C.; Barone, V.; Cammi, R.; Cancès, E.; Cossi, M.; Menucci, B.; Pommelli, C. S. *Adv. Quantum Chem.* **1998**, *32*, 227.
(33) Cancès, E.; Mennucci, B.; Tomasi, J. *J. Chem. Phys.* **1997**, *107*, 3032.
(34) Mennucci, B.; Cancès, E.; Tomasi, J. *J. Phys. Chem. B* **1997**, *101*, 10506.
(35) Klamt, A.; Schüürmann, G. *J. Chem. Soc., Perkin Trans. 2* **1993**, 799.
(36) Klamt, A.; Jonas, V. *J. Chem. Phys.* **1996**, *105*, 9972.
(37) Truong, T. N.; Stefanovich, E. V. *J. Chem. Phys.* **1995**, *103*, 3709.
(38) Truong, T. N. *Int. Rev. Phys. Chem.* **1998**, *17*, 525.
(39) Pullman, B.; Miertius, S.; Perahia, D. *Theor. Chim. Acta* **1979**, *50*, 317.
(40) Warshel, A.; Weiss, R. M. *J. Am. Chem. Soc.* **1980**, *102*, 6218.
(41) Hwang, J.-K.; King, G.; Creighton, S.; Warshel, A. *J. Am. Chem. Soc.* **1988**, *110*, 5297.
(42) Kelly, C. P.; Cramer, C. J.; Truhlar, D. G. *J. Phys. Chem. A* **2006**, *110*, 2493−2499.
(43) Rao, C. N. R.; Singh, S.; Senthilnathan, V. P. *Chem. Soc. Rev.* **1976**, *5*, 297.
(44) Linder, B. *J. Phys. Chem.* **1992**, *96*, 10708.
(45) Olivares del Valle, F. J.; Tomasi, J. *J. Chem. Phys.* **1987**, *114*, 231.
(46) Olivares del Valle, F. J.; Aguilar, M.; Tolosa, S.; Contador, J. C.; Tomasi, J. *J. Chem. Phys.* **1990**, *143*, 371.
(47) Aguilar, M. A.; Olivares del Valle, F. J.; Tomasi, J. *J. Chem. Phys.* **1991**, *150*, 151.
(48) Wang, J. Boyd, R. J.; Laaksonen, A. *J. Chem. Phys.* **1996**, *104*, 7261.
(49) Stefanovich, E. V.; Truong, T. N. *J. Chem. Phys.* **1996**, *105*, 2961.
(50) Tajkhorshid, E.; Jalkanen, K. J.; Suhai, S. *J. Phys. Chem. B* **1998**, *102*, 5899.
(51) Frisch, M. J.; Trucks, G. W.; Schlegel, H. B.; Scuseria, G. E.; Robb, M. A.; Cheeseman, J. R.; Montgomery, J. A., Jr.; Vreven, T.; Kudin, K. N.; Burant, J. C.; Millam, J. M.; Iyengar, S. S.; Tomasi, J.; Barone, V.; Mennucci, B.; Cossi, M.; Scalmani, G.; Rega, N.; Petersson, G. A.; Nakatsuji, H.; Hada, M.; Ehara, M.; Toyota, K.; Fukuda, R.; Hasegawa, J.; Ishida, M.; Nakajima, T.; Honda, Y.; Kitao, O.; Nakai, H.; Klene, M.; Li, X.; Knox, J. E.; Hratchian, H. P.; Cross, J. B.; Bakken, V.; Adamo, C.; Jaramillo, J.; Gomperts, R.; Stratmann, R. E.; Yazyev, O.; Austin, A. J.; Cammi, R.; Pomelli, C.; Ochterski, J. W.; Ayala, P. Y.; Morokuma, K.; Voth, G. A.; Salvador, P.; Dannenberg, J. J.; Zakrzewski, V. G.; Dapprich, S.; Daniels, A. D.; Strain, M. C.; Farkas, O.; Malick, D. K.; Rabuck, A. D.; Raghavachari, K.; Foresman, J. B.; Ortiz, J. V.; Cui, Q.; Baboul, A. G.; Clifford, S.; Cioslowski, J.; Stefanov, B. B.; Liu, G.; Liashenko, A.; Piskorz, P.; Komaromi, I.; Martin, R. L.; Fox, D. J.; Keith, T.; Al-Laham, M. A.; Peng, C. Y.; Nanayakkara, A.; Challacombe, M.; Gill, P. M. W.; Johnson, B.; Chen, W.; Wong, M. W.; Gonzalez, C.; Pople, J. A. *Gaussian 03*, revision D.01, Gaussian, Inc.: Wallingford, CT, 2004.
(52) Ramprasad, R.; Schneider, W. F.; Hass, K. C.; Adams, J. B. *J. Phys. Chem. B* **1997**, *101*, 1940
(53) Rauhut, G.; Pulay, P. *J. Phys. Chem.* **1995**, *99*, 3093.
(54) Pople, J. A.; Scott, A. P.; Wong, M. W.; Radom, L. *Isr. J. Chem.* **1993**, *33*, 345.
(55) Bauschlicher, C. W. *Chem. Phys. Lett.* **1995**, *246*, 40.
(56) Scott, A. P.; Radom, L. *J. Phys. Chem.* **1996**, *100*, 16502.
(57) Willis, B. G.; Jensen, K. F. *J. Phys. Chem. A* **1998**, *102*, 2613.
(58) Levy, H. A.; Corey, R. B. *J. Am. Chem. Soc.* **1941**, *63*, 2095.
(59) Donohue, J. *J. Am. Chem. Soc.* **1950**, *72*, 949.
(60) Avdeef, A.; Brown, J. A. *Inorg. Chim. Acta* **1984**, *91*, 67.
(61) Bagyan, G. A.; Valeev, A. K.; Koroleva, I. K.; Soroka, N. V. *Russ. J. Inorg. Chem.* **1983**, *28*, 1142.
(62) Kamoun, S.; Kamoun, M.; Daoud, A.; Romain, F. *Spectrochim. Acta*, 1**991**, *47A*, 1051.
(63) Batista de Carvalho, L. A. E.; Lourenço, L. E.; Margues, M. P. M. *J. Mol. Struct.* **1999**, *482*−483., 639.
(64) Ghazanfar, S. A. S.; Edsall, J. T.; Myers, D. V. *J. Am. Chem. Soc.* **1964**, *86*, 559.
(65) Takeda, M.; Iavazzo, R. E. S.; Garfinkel, D.; Scheinberg, I. H.; Edsall, J. T. *J. Am. Chem. Soc.* **1958**, *80*, 3813.
(66) Garfinkel, D.; Edsall, J. T. *J. Am. Chem. Soc.* **1958**, *80*, 3823.
(67) Ghazanfar, S. A. S.; Myers, D. V.; Edsall, J. T. *J. Am. Chem. Soc.* **1964**, *86*, 3439.